Ring Resonator Lasers using Passive Waveguides and Integrated Semiconductor Optical Amplifiers

Dominik G. Rabus, *Member, IEEE*, Zhixi Bian, and Ali Shakouri, *Member, IEEE*

***Abstract*—We present a review of our work on ring lasers using passive waveguides and couplers (directional and multimode interference) integrated with semiconductor optical amplifiers (SOAs). Two architectures are given in this paper. The first architecture includes the SOA inside the ring cavity. The second architecture also known as ring resonator coupled laser, consists of passive ring resonators having SOAs in the bus waveguides. The increased photon lifetime in the cavity and the tunability of the ring response can be used to make compact, narrow linewith, and widely tunable lasers. Four-wave mixing applications are also addressed.**

***Index Terms*—Laser, optical amplifier, resonator, ring, semiconductor.**

I. Introduction

SEMICONDUCTOR ring lasers have been investigated in the past and have recently gained attention again because they can be readily integrated with other optoelectronic devices and do not require gratings or facets for optical feedback, which is one of the advantages of ring resonators [1]. Ring lasers avoid spatial hole burning by traveling wave operation, which results in single-mode operation and reduced sensitivity to feedback. Different types of active and passive coupling configurations have been used in ring resonator lasers including Y-splitters, directional couplers, and multimode interference couplers. The application of ring resonators as lasers has been demonstrated already some time ago. Recently, tt has again gained attention with the fact that combining ring resonators can enhance the tunability of ring lasers. Novel concepts have been proposed and realized using all active ring lasers and passive ring resonator coupled configurations with integrated semiconductor optical amplifiers (SOAs). In this paper, we summarize our results, which we have obtained for single-ring resonators with SOA inside the ring cavity and double ring resonator coupled lasers having SOAs in the bus waveguides serving as the gain medium and absorber.

The paper is organized as follows. Section II provides details on the fabrication of the devices, which is the same for both architectures. Section III focuses on the results obtained for single ring lasers with SOA, demonstrating single-mode operation, limited tunability, and wavelength conversion. Section IV presents the results achieved for double ring resonator coupled lasers demonstrating single-mode operation and an enhanced tunability utilizing the Vernier effect.

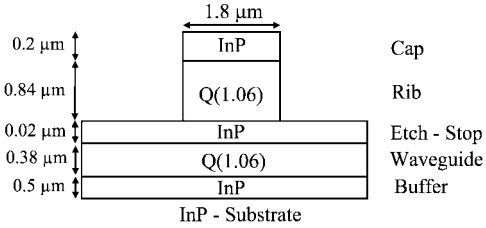

Fig. 1. Layer sequence and dimension of a passive waveguide.

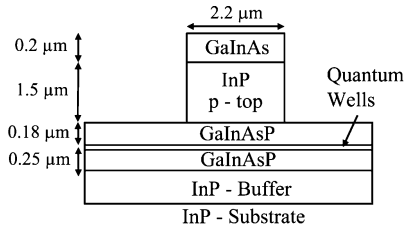

Fig. 2. Layer sequence and dimension of an SOA.

II. Fabrication

The layer sequence and the dimensions of the used waveguides, which have been used in [2] for realizing single, double, and triple ring resonator filters, are shown in Figs. 1 and 2.

The fabrication starts with the epitaxial growth of the SOA layers by using metal organic vapor phase epitaxy (MOVPE). The first chemical vapor deposition (CVD) processing step is the deposition of the SiN_x layer, which is ≈230 nm thick at a temperature of 370 °C for the fabrication of the etching mask. The lateral active mesa structures are defined in a resist pattern by using standard photolithography (positive process, photoresist AZ5214, exposing time ≈24 s, developer MFI724, developing time ≈50 s). The resist pattern serves as an etching mask for the following reactive-ion etching (RIE) step (CHF_3 22 sccm and O_2 2.2 sccm, pressure = 0.012 mbar, power = 50 W). The photoresist is removed with an O_2 plasma (10 min, power = 500 W, $T < 250\,^{\circ}C$) after this process. The p-top mesa are etched in the following step by using RIE (CH_4 8 ml/min and H_2 20 ml/min, pressure = 0.006 mbar, power = 200 W). In order to remove the polymer, which is formed during RIE, an O_2 plasma (20 min, power = 550 W, $T < 250\,^{\circ}C$) and a solution of KOH (20%) are used. The p-top is etched down to a distance of about 1.1–1.2 μm followed by a wet-etching step by using a solution of 20 H_2O:5 HBr:H_2O_2. This wet-etching process is the "undercut" etching. In this step, part of the sidewall is removed. A layer of InP protects the active sections underneath. The etching

Manuscript received October 30, 2006; revised July 31, 2007. The work of D. G. Rabus was supported by Alexander von Humboldt Foundation (www.avh.de) and the Baskin School of Engineering, University of California at Santa Cruz. The work of A. Shakouri was supported by the NSF CAREER and the Packard Foundation.

The authors are with Baskin School of Engineering, University of California at Santa Cruz, Santa Cruz, CA 95064 USA (e-mail: rabus@soe.ucsc.edu; zxbian@soe.ucsc.edu; ali@soe.ucsc.edu).

Digital Object Identifier 10.1109/JSTQE.2007.906043

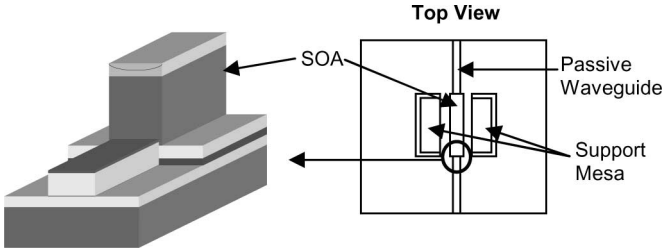

Fig. 3. Etching of the waveguide and the SOA.

of the undercut is indispensable for the second epitaxial growth step of the passive waveguide. The undercut reduces the formation of high "rabbit ears" during selective area MOVPE at the vicinity of the mask, and enables adequate control of the layer thickness in order to achieve the necessary vertical alignment within the active–passive transition. For further improvement of the selective area MOVPE (SAMOVPE) growth step, the "undercut" is covered by a layer of SiN_x, which is realized by depositing the entire wafer with SiN_x and removing the material on the bottom of the wafer by RIE, leaving the sidewalls covered. The next step is the final etching of the p-top and the active layers using RIE (CH_4 8 ml/min and H_2 20 ml/min, pressure $= 0.006$ mbar, power $= 200$ W). The control of the etch depth is very important in order to adjust the regrowth of the passive material. The following step is the regrowth of the passive material using SAMOVPE. The correct height of the passive material is defined by the thickness of an InP buffer layer. The regrowth process is followed by the removal of the entire SiN_x at the "undercut" using hydrofluoric acid (HF 5%). After this step, the entire wafer is covered again with a SiN_x layer ($\approx$190 nm) at a temperature of $370\,^{\circ}$C. The SiN_x is removed at the top of the active mesa using a photolithographic step, followed by a dry-etching step (CHF_3 22 sccm and O_2 2.2 sccm, pressure $= 0.012$ mbar, power $= 50$ W). The photoresist is removed after the dry-etching step using KOH (20%). The following diffusion process ($T = 575\,^{\circ}$C, 18 s) is carried out using zinc arsenide as the dopand. In the next step, the waveguide is etched together with the laser ridge in a so-called self-aligning process where the active–passive interface is generated using RIE (CH_4 6 ml/min, H_2 40 ml/min, O_2 0.3 ml/min, pressure $= 0.02$ mbar, power $= 150$ W). Due to the larger height of the laser ridge, the remaining material is etched by selective wet chemical etching using a solution of HCl and H_3PO_4 (1:4). The wet etching is automatically stopped when the quaternary layers are reached. The etching of the waveguide and the SOA is shown in Fig. 3.

The deep etching of the passive waveguide, which is necessary in order to achieve sufficient optical confinement in small bent waveguides (radii <200 μm), is the next processing step. The etching mask material is again an SiN_x layer structured in a photolithographic and dry-etching step. The SiN_x layer also serves as a protection layer for the laser ridge. The deep etching of the passive waveguide is done by RIE using CH_4 (8 ml/min) and H_2 (20 ml/min) with a pressure of 0.006 mbar and a power of 200 W. The SiN_x, which was deposited for the protection of the SOA ridge, has to be removed only at the very top of it to be able to place a metal layer for realizing an electric contact. Therefore, the entire wafer is covered with photoresist and is

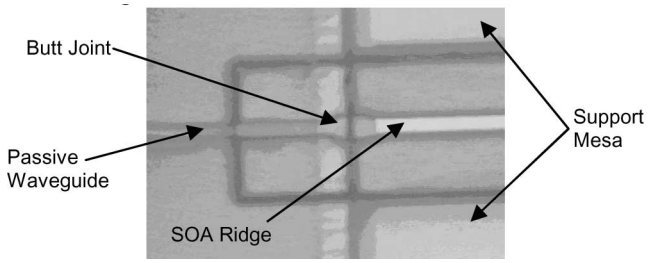

Fig. 4. Photograph of the removal of the photoresist at the top of the SOA ridge.

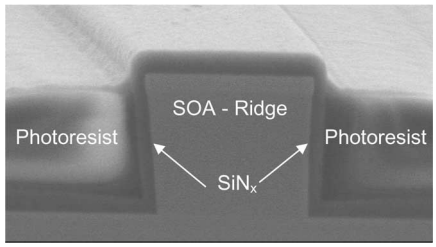

Fig. 5. SEM picture of the front view of an SOA ridge.

exposed for a few seconds ($\approx$14 s) at the areas of the SOA ridge, which results in opening the tip of the laser ridge. The photograph of the top view of an SOA ridge with the structured photoresist is shown in Fig. 4.

In this process, the exposing time of the photoresist is the key figure. If the time is too high, the photoresist will become very thin between the SOA ridge and the support mesa, and might uncover the insulating SiN_x layer, which will be etched in the next fabrication step and so cause unwanted shortcuts. On the other hand, if the exposing time is too short, only part of the photoresist on top of the SOA ridge is removed, and the SiN_x layer cannot entirely be etched away in the following process. The SiN_x layer at the top of the SOA ridge is completely free of photoresist. The area in between the SOA ridge and the support mesa and also the entire wafer are covered by photoresist with a thickness of about 800 nm, which is a sufficient amount for protecting the SiN_x layer from being etched in the next step. The SEM photograph of the cross section of a developed SOA ridge is shown in Fig. 5.

The SiN_x is removed from the p-top in a dry-etching process (CHF_3 24 sccm, H_2 1 sccm, pressure $= 0.012$ mbar, power $= 50$ W). Now, the metal contacts are fabricated starting with a photolithographic step for the definition of the contacts. The p-top of the SOA, the area in between the ridge and the support mesa and the top of the support mesa is deposited with titanium, platinum, and gold, and the remaining metal is removed in a "lift off" process using n-methyl-2-pyrrolidon (NMP); C_5H_9NO. An in-depth flow chart of the different stages of the integration process has been described in detail in [3].

III. Ring Lasers With an SOA Inside the Cavity

A. Introduction

One of the first integration of an SOA with passive silica waveguides and coupler is demonstrated in [4]. The gain in the ring resonator consists of a GaInAsP buried heterostructure

SOA. The facets of the SOA are coated with antireflecting films made from SiO. Both facets of the SOA are coupled to lensed optical fibers with a lens radius of 7 μm. The SOA module is inserted into the passive integrated silica ring resonator using etched fiber grooves. The size of the module is 1.2 mm $\times$ 1.2 mm $\times$ 3 mm. The fibers are fixed to the passive waveguides using a UV curable resin. The total resonator length is 10.2 cm, leading to a free spectral range (FSR) of 2 GHz at a wavelength of 1.3 μm. A comb-like lasing spectrum is obtained with a threshold current of only 17 mA. The device is temperature stabilized with a Peltier cooler.

An active resonator with passive Y-coupler and outcoupling waveguides has been realized in the material system InGaAs-GaAs in [5]. The ring laser is made out of strained-layer InGaAs-GaAs buried heterostructure waveguides. The integration of the passive Y-coupler is made by selective area growth. The radius of the ring laser is 200 μm. The facets are antireflection coated to avoid back reflections. The laser operates at a wavelength of around 1 μm with a threshold current of 25 mA. A side mode suppression of 24 dB is achieved.

Passive circular sections, an SOA, and a saturable absorber in the material system GaInAsP are used in [6] to fabricate a modelocked ring laser. The radius of the curved sections is 100 μm. Modelocking at frequencies of 29.5, 41.2, and 61.7 GHz is obtained for three different devices with corresponding SOA lengths of 1000, 650, and 300 μm and saturable absorber lengths of 30, 20, and 20 μm, respectively. A multimode interference (MMI) coupler is used for output coupling.

Ring lasers with MMI output couplers have been shown to have more superior operation characteristics as compared to devices with Y-junction couplers. A further improvement in performance of MMI coupled ring lasers, as suggested in [7] where completely active devices are presented, is by the use of a single active gain section in the ring, and making the MMI coupler and outcoupling waveguides of passive waveguide material as presented in this paper.

B. Single-Mode Operation

The performance of a racetrack-shaped ring resonator laser employing an SOA as the gain element having a length of 500 μm, where the input and output waveguides, the MMI coupler, and the curved ring sections are made out of passive material is described in the following paragraph. The passive waveguide is made from quaternary GaInAsP with a bandgap wavelength of 1.06 μm. The ring radius is 117 μm. The length of the MMI coupler is 150 μm. A photograph of a ring laser with integrated SOA is shown in Fig. 6. The butt coupling losses have been determined to be <2 dB each. The facets of the input and output waveguides have been antireflection coated. The ring laser has been designed to have an FSR of 50 GHz. The ring laser is operated at $T = 17\,^{\circ}$C. The lasing spectrum was measured using a tapered fiber and an optical spectrum analyzer (OSA).

The relationship between the lasing power in the fiber and the injection current in the SOA is shown in Fig. 7.

The threshold current is, as can bee seen from Fig. 7, as low as 25 mA. The kinks in the L–I curve of the ring laser are

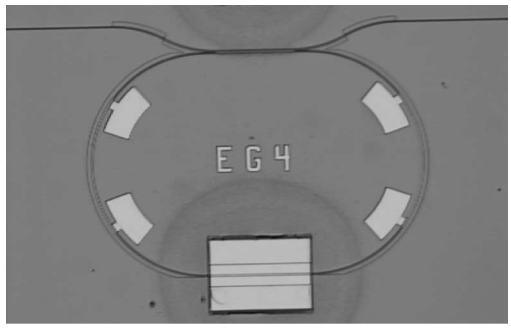

Fig. 6. Photograph of a ring resonator laser with integrated SOA.

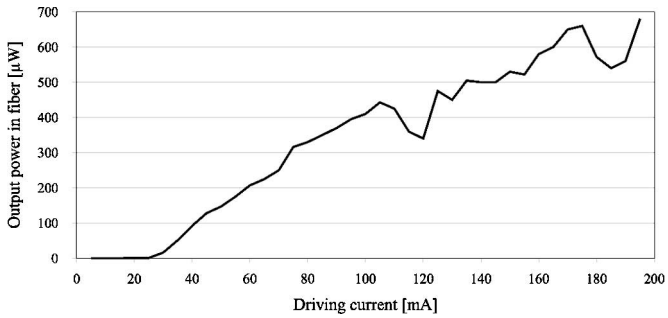

Fig. 7. Output power characteristic of a racetrack laser.

accompanied by mode hops and can be explained by coupled cavity effects, the second cavity being formed by the output path, which includes the MMI coupler [8]. The kinks have also been observed for fabricated ring lasers, which do not have an antireflection coating on the facets of the outcoupling waveguides. The SOA does not form a cavity with the butt joints. This has been verified by using a straight waveguide with integrated SOA where the input and output waveguides have been antireflection coated. No lasing has been observed in such a device with a 500 μm SOA. An interesting feature observed was that the same threshold current of 25 mA is obtained for a device, which was not antireflection coated.

The lasing spectrum of the racetrack laser at a drive current of 162 mA is shown in Fig. 8. An Advantest OSA Q8384 with a maximum resolution of 10 pm in this wavelength range is used. The measured full-width at half-maximum (FWHM) is, therefore, smaller than 1.25 GHz. The total power in the fiber is 0.6 mW/facet. As can be seen from the lasing spectra, the side mode suppression ratio (SMSR) is > 45 dB. The spectrum shows the designed FSR of 50 GHz of the ring resonator corresponding to 0.4 nm at a wavelength of 1.55 μm.

The lasing spectra covering the entire 50 nm gain spectrum is shown in Fig. 9. It can be clearly seen that there is only one lasing mode.

Ring resonators with integrated SOAs can also be used as optical filters depending on the current injected into the SOA. Fig. 10 shows the change in the transmission spectrum from a notch filter characteristic to an emission spectrum. The driving current used for the SOA is 27 and 34 mA, respectively.

Ring lasers fabricated by a combination of active and passive waveguide sections enable the lowering of the threshold current

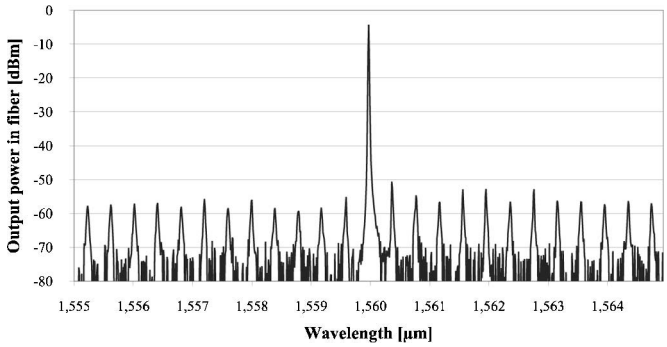

Fig. 8. Lasing spectra of a racetrack laser at a drive current of 162 mA, showing single-mode operation with SMSR = 45 dB.

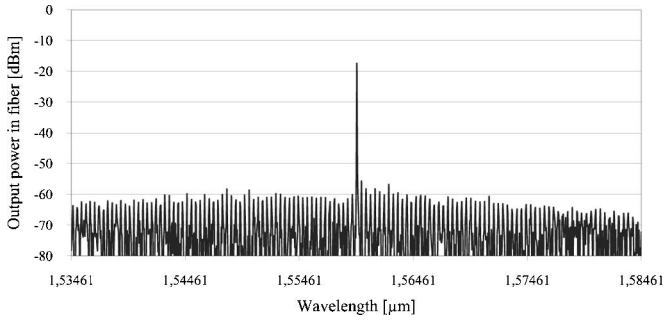

Fig. 9. Lasing spectrum of a racetrack laser showing single-mode operation over a 50 nm gain spectrum.

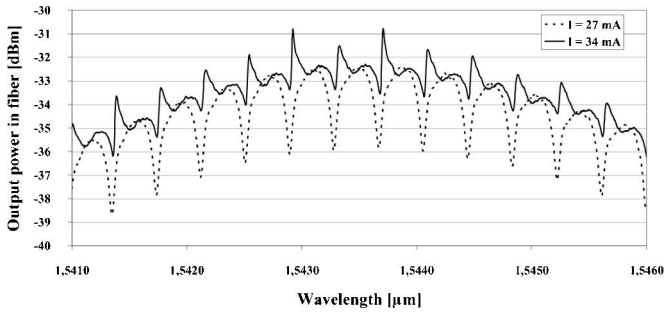

Fig. 10. Change from filter transmission to lasing.

as compared to all active devices, where the whole structure needs to be electrically contacted. Special attention has to be made when joining active and passive elements. Mode field profiles of both waveguides have to match as close as possible to minimize transition losses.

C. Tunability

The tuning of a single ring resonator laser via integrated platinum resistors [9] is limited to approximately 0.1 nm as shown in Fig. 11, which is insufficient for practical applications. Another possibility would be to heat or cool the entire chip as is done with most distributed feedback (DFB) lasers. Tunability is greatly enhanced using a double ring resonator configuration, as will be demonstrated in Section IV. The ohmic resistance of the platinum resistors is approximately 100 Ω each.

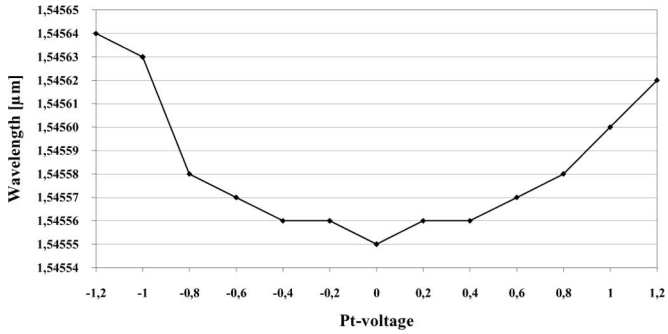

Fig. 11. Tuning of a ring laser using integrated Pt-resistors.

D. Wavelength Conversion

The four-wave mixing (FWM) effect can be applied to passive and active ring resonators, enabling efficient wavelength conversion for all-optical communication systems. Ring resonators based on GaAs or InP combine both advantages of a high nonlinear susceptibility and a high linear gain. In contrast to other active resonant structures like DFB lasers or SOAs, ring resonators enhance both the optical power of the signal wavelength at frequency ω_S as well as that of the converted wavelength at ω_C. Maximum conversion efficiency is achieved when ω_S and ω_C fit one of the resonance wavelengths of the ring resonator. No stopband has to be taken into account. Operating at wavelengths not being one of the resonance wavelengths of the ring resonator results in a reduced conversion efficiency. The internal optical field enhancement and the FSR can be designed by the radius and the power coupling ratio between the ring resonator and the bus waveguides.

A passive GaAs racetrack-shaped ring resonator is used in [10] to demonstrate wavelength conversion by FWM with an improved conversion efficiency compared to a straight waveguide. The properties of an all-optical wavelength converter with reshaping characteristics based on FWM in a passive GaAs–AlGaAs ring resonator notch filter are investigated in [11]. A detailed theoretical analysis of the static and dynamic reshaping characteristics of the wavelength converter is carried out. Improved conversion efficiency is expected in ring resonators fabricated as all-active ring resonators. An active ring resonator architecture used for wavelength conversion is demonstrated in [12].

Wavelength conversion can also be performed using passive ring resonators with integrated SOAs (Fig. 6) as the pump laser, and inserting a signal wavelength into the bus waveguide placed on a resonance of the ring resonator. The result of an FWM experiment using a racetrack-shaped ring resonator with an integrated SOA utilizing direct adjacent resonances is shown in Fig. 12. The ring resonator has a radius of 117 μm. A directional coupler with a gap of 1 μm and a length of 150 μm is used for coupling into and from the resonator. The overall FSR is 0.4 nm, which corresponds to 50 GHz at a wavelength of 1550 nm. A conversion efficiency of approximately -6 dB is achieved. The driving current for the SOA is 119 mA. The signal wavelength is inserted into the ring resonator from an external cavity laser (ECL), which is amplified by an erbium doped fiber amplifier (EDFA) to a total signal power of 3 mW.

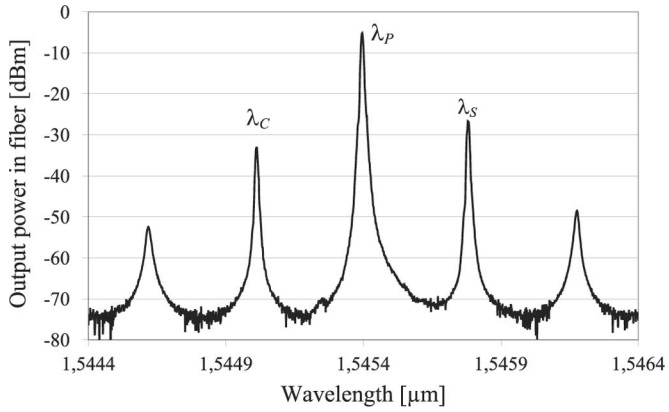

Fig. 12. FWM in a ring resonator with integrated SOA, using direct adjacent resonances.

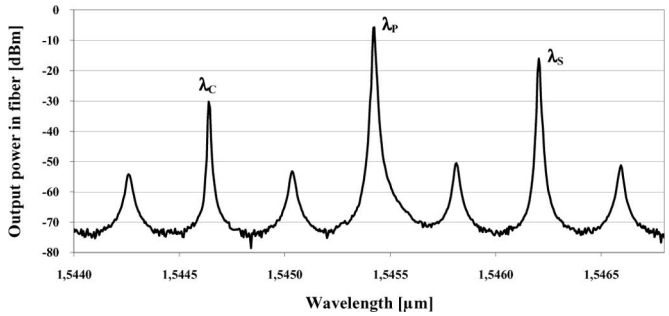

Fig. 13. FWM in a ring resonator with integrated SOA, using the second resonances next to the pump wavelength λ_p.

λ_P is the pump laser wavelength coming from the ring laser, λ_S is the signal wavelength, and λ_C is the converted wavelength. Another FWM experiment using resonances spaced further apart is shown in Fig. 13. Here, a conversion efficiency of only -14.2 dB is achieved, which is attributed to the wavelength spacing away from the pump wavelength. The highest conversion efficiency is achieved when a resonance is located directly next to the pump wavelength. Ring resonators are ideal candidates for wavelength conversion, as they can be designed to have the exact channel spacing used in wavelength division multiplexing (WDM) or dense WDM (DWDM) networks, assuring that the converted wavelength is located on a resonance wavelength also being a data channel. Channel spacing alignment is only possible for a few channels being next to each other and not the entire WDM grid, due to dispersion effects.

IV. Double Ring Resonator Coupled Lasers

A. Introduction

Ring resonator coupled lasers are different from the ring lasers in Section III as the gain medium is placed outside the ring resonator cavity (Fig. 14). Passive ring resonators serve as optical filters, which enable single-mode operation and tunability of the laser.

Ring resonator coupled lasers offer many promising advantages over conventional tunable lasers, including ultrawide wavelength tuning range, high SMSR, uniform threshold and efficiency, narrow linewidth, and low-frequency chirp. The integration of active gain sections, passive waveguides, and ring resonators forming a ring resonator coupled laser has recently been proposed and analyzed in [13]. A detailed analysis of a single passive ring resonator coupled laser is given in [14].

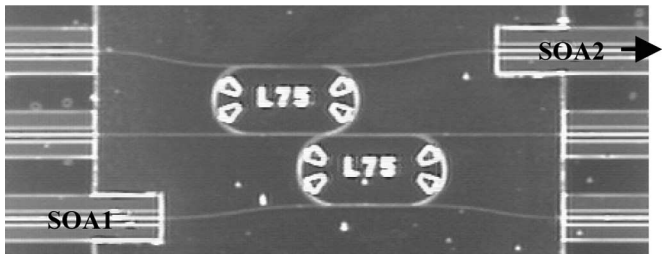

Fig. 14. Photograph of a DR-RCL.

One of the first fabricated passive single ring resonator coupled lasers is presented in [15]. The same material is used for the ring coupled laser. The ring is operated in a transparent mode. Only the waveguides at the facets introduce gain into the device. The waveguides not leading to the facets act as absorbers. The ring coupled laser is made using the material system GaInAsP on InP. Three types of devices having a radius of 5, 10, and 20 μm are fabricated. The width of the waveguides is 0.4 μm. Directional couplers with a coupling gap of 0.2 μm are used. The bus waveguides are tapered to a width of 2 μm having a taper length of 200 μm. The FSR of the ring resonator is chosen large enough such that a resonance is in the middle of the gain spectrum to achieve single-mode operation. The threshold of the laser is 70 mA under pulsed operation. The lasing wavelength is measured to be 1.549 μm.

In order to achieve single-mode operation, the radius of the ring resonator has to be small in the order of 10–20 μm. Another way to achieve single-mode operation using passive coupled ring resonators is by using a double ring architecture. A double ring resonator opens up the possibility of expanding the FSR to the least common multiple of the FSR of individual ring resonators. This is done by choosing different radii in the double ring resonator. In the case of different radii, the light passing through the double ring resonator is launched from the drop port when the resonant conditions of both single ring resonators are satisfied. The FSR of the double ring resonator with two different radii is expressed by

$$\mathrm{FSR} = N\mathrm{FSR}_1 = M\mathrm{FSR}_2 \tag{1}$$

which leads to

$$\mathrm{FSR} = |M - N| \frac{\mathrm{FSR}_1 \cdot \mathrm{FSR}_2}{|\mathrm{FSR}_1 - \mathrm{FSR}_2|} \tag{2}$$

where N and M are natural and coprime numbers. The use of two ring resonators with different radii opens the possibility to realize a larger FSR than would be achieved using only a single ring resonator.

Passive double ring resonator coupled lasers (DR-RCLs) are analyzed theoretically in [16].

A double ring coupled laser is demonstrated in [17] using an integrated tunable polymer double ring filter, fiber coupled to EDFA, serving as the gain medium. Thermooptic and electrooptic tunable devices are presented. The radii of the ring resonators

are 240 and 246 μm. The overall obtained FSR is approximately 39 nm at a wavelength of 1550 nm. One of the several advantages of using a double ring resonator is the possibility of a higher tuning enhancement factor using the Vernier effect. The tuning enhancement factor is given by

$$T = \frac{1}{1 - \frac{L_1}{L_2}} = \frac{R_2}{R_2 - R_1} \tag{3}$$

where L_1 and L_2 are the cavity lengths of each ring and R_1 and R_2 the radius, respectively. The tuning range of a double ring resonator is T times the tuning range of a single ring. The polymer double ring resonator configuration, e.g., has a tuning enhancement factor of 40. The transmission experiments are performed using TM polarized input light fed to the input port of the double ring resonator from an EDFA, which serves as the gain medium. An output power of 1 mW and an SMSR of 30 dB are measured for both the thermooptic and the electrooptic device.

One of the first integrated double ring resonator coupled lasers in GaInAsP combining passive ring resonators with integrated SOAs is presented in [18]. A photograph of a DR-RCL is shown in Fig. 14. The layer sequence and the dimensions of the waveguides are the same as is described in Section III for the passive ring resonator and the integration of an SOA into the ring cavity. The passive double ring resonators have slightly different circumferences (ring radii of 100 and 104 μm) so that the effective FSR of the double ring filter is much larger than that of single rings. Current is only applied to SOA1 and SOA2 having a length of 500 μm. The other active sections (length $=$ 300 μm) are used as absorbers. The light from the SOA section can propagate along the passive waveguide and couple into and out of the ring resonators via directional couplers. The bus waveguide-resonator coupling ratio is a key parameter determining the performance of the RCL, and there is a tradeoff between threshold current and linewidth [14]. The air gap and length of the directional coupler are 0.8 and 250 μm, respectively, which gives an estimated coupling ratio of 50%. The advantage of a large coupling ratio is small ring resonator transmission loss and a decrease of laser threshold current. The facets are as cleaved, providing room for further improvement of the optical characteristics in applying reflective and antireflective layers accordingly.

B. Single-Mode Operation

The spectrum of a DR-RCL (coupler length $=$ 500 μm, coupling gap $=$ 1 μm) with an FSR of 30 nm is shown in Fig. 15. An SMSR of $>$35 dB is obtained, which is limited by the dynamic range (-35 dB) of the used OSA. The linewidth of the lasing wavelength is also limited by the bandwidth of the OSA, which is 0.06 nm. From the calculations, the linewidth is estimated to be $<$2 MHz. The driving currents for SOA1 and SOA2 are 100 and 90 mA, respectively.

Fig. 16 shows the dependence of the output power of a slightly different DR-RCL (coupler length $=$ 250 μm, coupling gap $=$ 0.8 μm) on a bias current of SOA2 for different stage temperatures of 16, 18, and 22 °C, when the bias current of SOA1 is 94 mA. The threshold currents of SOA2 at these three stage temperatures are 20, 23, and 25 mA, respectively. It can also be

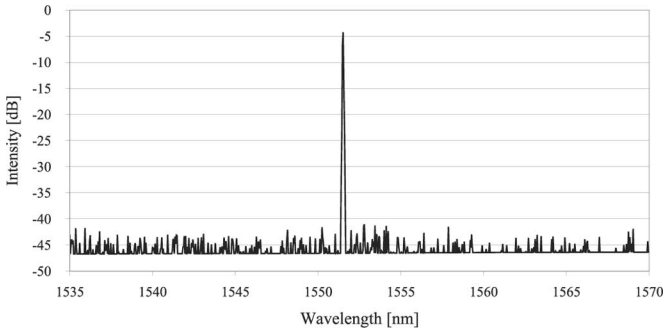

Fig. 15. Spectrum of a DR-RCL with an FSR of 30 nm.

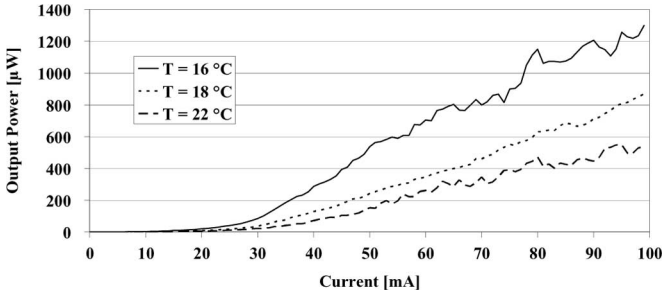

Fig. 16. Output power as a function of bias current of SOA2 for different stage temperatures of 16, 18, and 22 °C, when bias current of SOA1 is 94 mA.

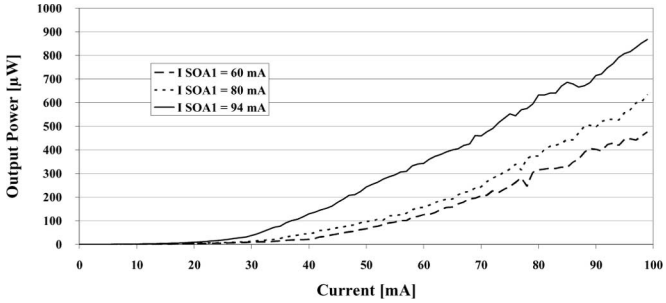

Fig. 17. Output power as a function of bias current of SOA2 for different bias currents of SOA1, when the stage temperature is 18 °C.

seen that the differential efficiency increases with the decrease of stage temperature. Fig. 17 compares the curves of output power as a function of bias current of SOA2 for different bias currents of SOA1 when the stage temperature is 18 °C. The bias current of SOA2 has more significant effects than bias current of SOA1 because the light power in the cavity is not uniform, and the output power is collected at SOA2 having a cleaved facet. However, the contribution from bias current of SOA1 shows that the laser cavity does include the two SOA sections and the double ring filter connecting them. The laser power of around 1 mW is not as high as expected. Although it is very difficult to locate the cavity loss sources, the IR imaging and theoretical analysis indicate that the largest loss is mainly at the transition between passive bus waveguide and SOA sections.

C. Tunability

The resonance wavelength of the rings can be tuned by the integrated platinum resistors on top of the passive waveguides in the ring resonators. Varying the current of one heater results

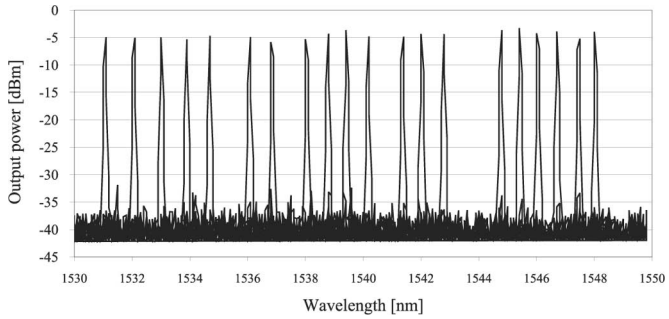

Fig. 18. Wavelength tuning by applying a current between 0 and 30 mA to the integrated Platinum heater.

in a shift of resonance wavelength of the corresponding ring resonator due to the thermooptic effect, and the lasing can jump from one mode to the next one where the transmission peaks of the double ring resonators overlap. Fig. 18 shows a series of lasing spectra obtained from a DR-RCL having a coupler length of 250 μm and a coupling gap of 0.8 μm when varying the heater current between 0 and 30 mA. When the current of the integrated heater is changed, the laser produces 20 different modes, which are spread uniformly over a 17 nm wavelength range. Recently [19], a tuning range of 30 nm has been achieved for a DR-RCL by using current injection.

A side mode suppression of 30 dB is achieved for the 20 discrete modes. The lasing quality and wavelength tuning can be improved if the cavity loss is reduced in a further development.

V. Conclusion

Ring-resonator-based lasers utilizing two different architectures employing passive waveguides and couplers integrated with SOAs have been presented, demonstrating their application as narrow linewidth single-mode lasers and wavelength converters in future all- optical networks. Double ring resonator coupled lasers are especially suited as tunable lasers offering a wide tuning range and a high SMSR.

Acknowledgment

The authors would like to thank R. Steingrüber and C. Weimann (for mask fabrication), H. Schroeter-Janssen (for SAMOVPE), F. Reier and H. Barsch (for epitaxy), I. Tiedke, Ch. Schultz, B. Reinsperger (for photolithography), and R. Schmidt and R. Tuerck (for antireflection coating). D. G. Rabus would like to thank H. Heidrich, M. Hamacher, and U. Troppenz for their overwhelming support.

References

[1] D. G. Rabus, *Integrated Ring Resonators, Springer Series in Optical Sciences*. Berlin, Heidelberg, New York: Springer, 2007.

[2] D. G. Rabus, M. Hamacher, U. Troppenz, and H. Heidrich, "Optical filters based on ring resonators with integrated semiconductor optical amplifiers in GaInAsP/InP," *IEEE J. Select. Topics Quantum Electron.*, vol. 8, no. 6, pp. 1405–1411, Nov./Dec. 2006.

[3] D. G. Rabus, "Realization of optical filters using ring resonators with integrated semiconductor optical amplifiers in GaInAsP/InP," Ph.D. dissertation, Department of Electrical Engineering and Computer Science, Technical University Berlin, Der Andere Verlag, 2002.

[4] Y. Hibino, H. Terui, A. Sugita, and Y. Ohmori, "Silica-based optical waveguide ring laser integrated with semiconductor laser amplifier on Si substrate," *Electron. Lett.*, vol. 28, no. 20, pp. 1932–1933, Sep. 1992.

[5] T. M. Cockerill, M. L. Osowski, R. M. Lammert, and J. J. Coleman, "A strained-layer InGaAs-GaAs buried heterostructure circular ring laser with integrated y-coupled passive waveguide by selective-area metalorganic chemical vapor deposition," in *Proc. ISLC*, 1994, pp. 195–196.

[6] T. Ohno, H. Ishii, S. Matsuo, H. Okamoto, Y. Kawaguchi, Y. Kondo, T. Furuta, H. Ito, and Y. Yoshikuni, "Hybrid modelocking of semiconductor ring lasers incorporating passive deep-ridge waveguides," *Electron. Lett.*, vol. 38, no. 16, pp. 884–886, Aug. 2002.

[7] E. C. M. Pennings, R. van Roijen, M. J. N. van Stralen, P. J. de Waard, R. G. M. P. Koumans, and B. H. Verbeek, "Reflection properties of multimode interference devices," *IEEE Photon. Technol. Lett.*, vol. 6, no. 6, pp. 715–718, 1994.

[8] T. F. Krauss, R. M. De, La Rue, P. J. R. Laybourn, B. Vogele, and C. R. Stanley, "Efficient semiconductor ring lasers made by a simple self-aligned fabrication process," *IEEE J. Sel. Topics Quantum Electron.*, vol. 1, no. 2, pp. 757–761, Jun. 1995.

[9] D. G. Rabus, M. Hamacher, and H. Heidrich, "Resonance frequency tuning of a double ring resonator on GaInAsP/InP: Experiment and simulation," *Jpn. J. Appl. Phys.*, vol. 41, pt 1, no. 2B, pp. 1186–1189, Feb. 2002.

[10] P. P. Absil, J. V. Hryniewicz, B. E. Little, P. S. Cho, R. A. Wilson, L. G. Joneckis, and P. T. Ho, "Wavelength conversion in GaAs microring resonators," *Opt. Lett.*, vol. 25, no. 8, pp. 554–556, 2000.

[11] S. Mikroulis, A. Bogris, E. Roditi, and D. Syvridis, "Investigation of an all-optical wavelength converter with reshaping properties based on four-wave mixing in passive microring resonators," *IEEE J. Lightw. Technol.*, vol. 22, no. 12, pp. 2743–2746, Dec. 2004.

[12] M. Hamacher, U. Troppenz, H. Heidrich, and D. G. Rabus, "Active ring resonators based on GaInAsP/InP," *Proc. SPIE*, vol. 4947, pp. 212–222, 2003.

[13] B. Liu, A. Shakouri, and J. E. Bowers, "Passive microring-resonator-coupled lasers," *Appl. Phys. Lett.*, vol. 79, no. 22, pp. 3561–3563, 2001.

[14] Z. Bian, B. Liu, and A. Shakouri, "InP-Based passive ring-resonator-coupled lasers," *IEEE J. Quantum Electron.*, vol. 39, no. 7, pp. 859–865, Jul. 2003.

[15] S. Park, S. S. Kim, L. Wang, and S. T. Ho, "Single-mode lasing operation using a microring resonator as a wavelength selector," *IEEE J. Quantum Electron.*, vol. 38, no. 3, pp. 270–273, Mar. 2002.

[16] B. Liu, A. Shakouri, and J. E. Bowers, "Wide tunable double ring resonator coupled lasers," *IEEE Photon. Technol. Lett.*, vol. 14, no. 5, pp. 600–602, May 2002.

[17] P. Rabiei and W. H. Steier, "Tunable polymer double micro-ring filters," *IEEE Photon. Technol. Lett.*, vol. 15, no. 9, pp. 1255–1257, Sep. 2003.

[18] D. G. Rabus, Z. Bian, and A. Shakouri, "A GaInAsP/InP double ring resonator coupled laser," *IEEE Photon. Technol. Lett.*, vol. 17, no. 9, pp. 1770–1772, Sep. 2005.

[19] S. Matsuo, T. Segawa, T. Kakitsuka, H. Okamoto, Y. Kawaguchi, Y. Kondo, H. Suzuki, and Y. Yoshikuni, "Widely tunable laser using microring resonators," in *Proc. Semicond. Laser Conf.*, 2006, pp. 21–22.

Dominik G. Rabus (M'02) received the Dipl.-Ing. degree in electrical engineering and computer sciences from the University of Stuttgart, Stuttgart, Germany, in 1999 and the Dr.-Ing. degree in electrical engineering and computer sciences from the Technical University of Berlin, Berlin, Germany, in 2002.

After working with the Fraunhofer Institute for Telecommunications, Heinrich-Hertz-Institut, Berlin, on ring resonators on InP, he joined the Institute for Microstructure Technology, Forschungszentrum Karlsruhe, Karlsruhe, Germany, in 2003, where he worked on polymer-waveguide-based devices. Since 2006, he has been with the Baskin School of Engineering, University of California, Santa Cruz, working on biophotonic devices.

Dr. Rabus received the Feodor–Lynen Fellowship from Alexander von Humboldt Foundation, Bonn, Germany, in 2006. He has been the Chairman of the topics Optofluidics: Emerging Technologies and Applications, and Imprinting of Photonic Integrated Circuits at the IEEE/LEOS Summer Topicals 2006 and 2007, respectively. Since 2007, he has been the IEEE LEOS Topicals General Chair for the annual conference series of IEEE LEOS Summer and Winter Topicals.

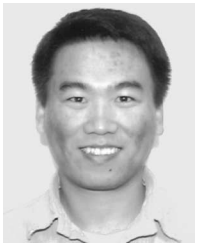

Zhixi Bian received the B.S. degree in electronics from Nankai University, Tianjin, China, in 1993, the M.S. degree in electronics from Beijing University, Beijing, China, in 1996, and the Ph.D. degree from the University of California, Santa Cruz, in 2004.

He is currently a Postdoctoral Researcher with the University of California, Santa Cruz. His research interests include tunable semiconductor lasers, optoelectronic and photonic integrated circuits, carrier transport in micro- and nanodevices, renewable energy, and thermoelectric cooling.

Ali Shakouri (M'01) received the Ph.D. degree in electrical engineering from California Institute of Technology, Pasadena, in 1995.

He is currently a Professor of electrical engineering with the University of California, Santa Cruz (UCSC), where he is also the Director of the Thermionic Energy Conversion Center. His current research interests include nanoscale heat and current transport in semiconductor devices, submicron thermal imaging, and microrefrigerators on a chip and novel optoelectronic integrated circuits.

Dr. Shakouri received the Packard Fellowship in Science and Engineering in 1999, the National Science Foundation Career Award in 2000, and the UCSC School of Engineering First Professor Award in 2004.